FORMULATION AND INTERPRETATION OF OPTIMAL BRAKING PATTERNS IN AUTONOMOUS LANE-KEEPING MANEUVERS

Victor Fors
Björn Olofsson
Lars Nielsen
Division of Vehicular Systems,
Department of Electrical Engineering,
Linköping University,
Sweden
E-mail: `victor.fors@liu.se`

ABSTRACT

The two perspectives of autonomous driving and new active safety in vehicles are complementary, and both hold promise to reduce the number of accidents and associated severe or fatal injuries. They both coincide in the recent interest in finding alternatives to traditional yaw-control systems that can utilize the full potential of the vehicle. By considering the control problem as that of lane-keeping, also at high speed and at-the-limit of tire friction, rather than that of yaw control, leads to the possibility of optimization-based active-braking systems with better performance than those existing today. Here, we investigate the optimal braking patterns in completely autonomous lane-keeping maneuvers resulting from a formulation where the optimization criterion used is an interpolation between the initial and final velocities of the maneuver. Varying the interpolation parameter, *i.e.*, the relative weight between the initial and final velocity, results in different vehicle behavior. The analysis of these behaviors provides several new insights into stabilizing braking patterns for vehicles in at-the-limit maneuvers. Specifically, it is to be noted that the benefits of a lane-keeping strategy are immediate, both in terms of the maximum possible initial velocity and the velocity reduction. The formulation embeds the traditional yaw control and optimal lane-keeping as the end-point values of the interpolation parameter, and adds a continuous family of behaviors in between. This gives a new perspective for investigating the relation between traditional yaw control and optimal lane-keeping for autonomous vehicles.

1 INTRODUCTION

Active-safety and driver-assistance systems are fundamental components in modern passenger cars as well as trucks. Common examples include the anti-lock braking system (ABS) and the electronic stability control (ESC) systems [1]. The latter could be achieved by yaw control of the vehicle, *i.e.*, by inducing appropriate braking on the wheels in order to try to stay on the road when vehicle maneuverability is lost. An illustrative situation in which maneuverability may be lost and ESC systems are of importance is when entering a turn with a velocity that is too high for the driver to maintain controllability as a result of the maximum tire forces that can be developed.

There is now a strong trend toward autonomous driving, and on the path to full autonomy of the vehicle partial autonomous functions or active-safety systems are included in the vehicle so as to reduce the number of accidents and associated severe or fatal injuries. Recently, there has been an increased interest in finding alternatives to traditional yaw-control systems that can utilize the full potential of the vehicle, and in particular the available tire forces, in critical situations where the vehicle should perform at the limit. By considering the control problem as that of lane-keeping rather than that of yaw control, several interesting perspectives open up. More specifically, utilizing the increasingly powerful onboard sensor and computation systems in the car, information about the road and traffic ahead could be extracted and used for keeping the vehicle on the road. Ultimately, this would then enable optimization-based active-safety systems executing online in the vehicle.

In [2], we started an analysis of the possible benefits of increased situation awareness and autonomous optimization-based stability control systems for vehicles. In that paper, the focus was to quantify the maximum initial velocity that could be handled in a left-hand turn, both with optimal active yaw-control systems and an optimal lane-keeping controller (both including optimal steering angles, assuming complete autonomy without human intervention). The evaluation was performed using several different situations, which differed in terms of turn geometry and road conditions. In [3], different actuator configurations of a vehicle were examined by quantifying the maximum initial velocity that could be handled, using similar scenarios as those considered in this paper. In [4], a comparison of the optimal maneuvers in a turn with the criteria of minimum time and maximum exit velocity, respectively, was presented using an optimal-control approach. Related research was also presented in [5], where a similar critical maneuvering situation in a turn was investigated and a control law referred to as the parabolic path reference strategy was proposed and shown to result in good performance when evaluated in a semi-autonomous scenario employing a double-track vehicle model compared to conventional yaw control. Thus, the interest in and potential of lane-keeping stability control is high.

In this paper, we present an analysis that extends the results in [2] and is complementary to [5]. We investigate the optimal braking patterns in completely autonomous lane-keeping maneuvers in several relevant scenarios. More specifically, the optimal braking and steering maneuvers in a left-hand turn, a double lane-change scenario, and an avoidance-maneuver situation are computed and analyzed in the light of future autonomous safety systems. Several interesting common behavior is observed for the maneuvers in the different situations when studying the optimal solutions in detail, which holds promise for the future practical applicability of the presented results. This analysis, with the perspective of lane keeping, turns out to, with a simple parameterization of the cost function as a linear combination of the initial and final velocities, provide several new insights into the relation between different braking patterns for vehicles in at-the-limit maneuvers.

2 MODELING

The vehicle model is based on a double-track chassis model with both longitudinal and lateral load transfer according to [6] and a nonlinear tire-force model using the Pacejka's Magic Formula with weighting functions for modeling the forces under combined longitudinal and lateral wheel slip [7]. As a particular feature, wheel dynamics is included in the model and the inputs are therefore considered as the wheel torques directly in favor of the longitudinal tire forces. This has been found advantageous [8], since this is the quantity that could be controlled in a physical vehicle. The complete model of the dynamic system can be written with the following 23 states x and 5 inputs u:

$$x = \begin{bmatrix} [X_p, Y_p, \psi]^T \\ [v_x, v_y, r]^T \\ [\phi, \dot{\phi}, \theta, \dot{\theta}]^T \\ \delta \\ [T_1, T_2, T_3, T_4]^T \\ [\alpha_1, \alpha_2, \alpha_3, \alpha_4]^T \\ [\omega_1, \omega_2, \omega_3, \omega_4]^T \end{bmatrix}, \quad u = \begin{bmatrix} \dot{\delta} \\ T_{u,1} \\ T_{u,2} \\ T_{u,3} \\ T_{u,4} \end{bmatrix}, \tag{1}$$

whose relations are described in the following subsections.

2.1 World Model

The vehicle traverses in a global coordinate system with position (X_p, Y_p), and orientation ψ according to

$$\dot{\psi} = r, \tag{2}$$

$$\dot{X}_p = v_x \cos(\psi) - v_y \sin(\psi), \tag{3}$$

$$\dot{Y}_p = v_x \sin(\psi) + v_y \cos(\psi), \tag{4}$$

where the vehicle states are defined in Figure 1 with the angular velocity r, the longitudinal velocity v_x, and the lateral velocity v_y.

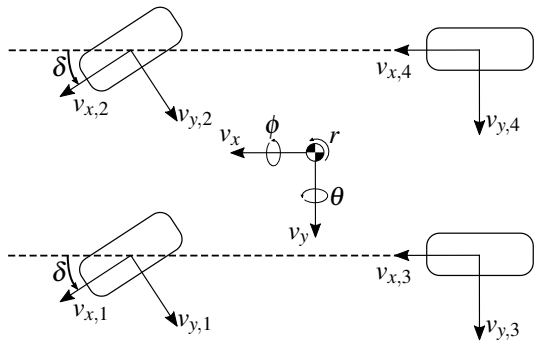

Figure 1. Double-track vehicle model.

2.2 Wheel and Tire Model

Counted from the front left wheel to the rear right wheel, the vehicle has four wheels denoted with subscript $i \in \{1,2,3,4\}$. The velocity of each wheel in their local coordinate system, $(v_{x,i}, v_{y,i})$, is described by

$$\begin{bmatrix} v_{x,i} \\ v_{y,i} \end{bmatrix} = \begin{bmatrix} \cos(\delta_i) & \sin(\delta_i) \\ -\sin(\delta_i) & \cos(\delta_i) \end{bmatrix} \left(\begin{bmatrix} v_x \\ v_y \end{bmatrix} + r \begin{bmatrix} l_{y,i} \\ l_{x,i} \end{bmatrix} \right), \quad (5)$$

where subscript i denotes the corresponding wheel, δ_i is the wheel angle in relation to the chassis, and $(l_{x,i}, l_{y,i})$ is the position of the wheel relative to the vehicle center of mass. The angle of the two wheels on the front axle is defined by the steering angle δ according to $\delta_1 = \delta_2 = \delta$, while the angles of the back wheels are constant $\delta_3 = \delta_4 = 0$.

The wheel dynamics are given by

$$T_i = I_w \dot{\omega}_i + R_w F_{x,i}, \quad (6)$$

where T_i is the applied driving or braking torque of wheel i, I_w is the wheel inertia, R_w is the wheel radius, and $F_{x,i}$ is the longitudinal force from the tire traction. The braking of each wheel is individually actuated by an input torque $T_{u,i}$ through a first-order system

$$\gamma_T \dot{T}_i + T_i = T_{u,i}, \quad (7)$$

where γ_T is a time constant.

The slip angles α_i and slip ratios κ_i are defined according to [7],

$$\frac{\sigma}{v_{x,i}} \dot{\alpha}_i + \alpha_i = -\arctan(\frac{v_{y,i}}{v_{x,i}}), \quad (8)$$

$$\kappa_i = \frac{R_w \omega_i - v_{x,i}}{v_{x,i}}, \quad (9)$$

where σ is the relaxation length, R_w is the wheel radius, and ω_i is the angular velocity of the wheel. The longitudinal forces $F_{x,i}$ and lateral forces $F_{y,i}$ of the tires are modeled using Pacejka's Magic Formula with weighting functions [7] and are given by

$$\begin{aligned} F_{x0,i} &= \mu_{x,i} F_{z,i} \sin(C_{x,i} \arctan(B_{x,i}\kappa_i \\ &\quad - E_{x,i}(B_{x,i}\kappa_i - \arctan(B_{x,i}\kappa_i))), \quad (10) \\ H_{x\alpha,i} &= B_{x1,i} \cos(\arctan(B_{x2,i}\kappa_i)), \quad (11) \\ G_{x\alpha,i} &= \cos(C_{x\alpha,i} \arctan(H_{x\alpha,i}\alpha_i), \quad (12) \\ F_{x,i} &= G_{x\alpha,i} F_{x0,i}, \quad (13) \end{aligned}$$

$$\begin{aligned} F_{y0,i} &= \mu_{y,i} F_{z,i} \sin(C_{y,i} \arctan(B_{y,i}\alpha_i \\ &\quad - E_{y,i}(B_{y,i}\alpha_i - \arctan(B_{y,i}\alpha_i))), \quad (14) \\ H_{y\kappa,i} &= B_{y1,i} \cos(\arctan(B_{y2,i}\alpha_i)), \quad (15) \\ G_{y\kappa,i} &= \cos(C_{y\kappa,i} \arctan(H_{y\kappa,i}\kappa_i), \quad (16) \\ F_{y,i} &= G_{x\alpha,i} F_{y0,i}, \quad (17) \end{aligned}$$

where $F_{z,i}$ are the normal forces on each wheel, B, C and E are model parameters, and μ_x and μ_y are the friction coefficients.

2.3 Chassis Model

The force and moment equilibria are given by (see, *e.g.*, [6])

$$F_x = \sum_{i=1}^{4} F_{x,i} \cos(\delta_i) - F_{y,i} \sin(\delta_i), \quad (18)$$

$$F_y = \sum_{i=1}^{4} F_{x,i} \sin(\delta_i) + F_{y,i} \cos(\delta_i), \quad (19)$$

$$M_z = \sum_{i=1}^{4} \begin{bmatrix} l_{x,i} & l_{y,i} \end{bmatrix} \begin{bmatrix} F_{x,i} \sin(\delta_i) + F_{y,i} \cos(\delta_i) \\ F_{y,i} \sin(\delta_i) - F_{x,i} \cos(\delta_i) \end{bmatrix}. \quad (20)$$

A summary of the motion equations of the chassis, derived in [6] are given below. The reader is referred to the technical report for further details. The translational motion equations can be written as

$$\dot{v}_x - v_y r = \frac{F_x}{m} + f_x(r, \dot{r}, \phi, \dot{\phi}, \ddot{\phi}, \theta, \dot{\theta}, \ddot{\theta}), \quad (21)$$

$$\dot{v}_y + v_x r = \frac{F_y}{m} + f_y(r, \dot{r}, \phi, \dot{\phi}, \ddot{\phi}, \theta, \dot{\theta}, \ddot{\theta}), \quad (22)$$

where $f_x(\cdot)$ and $f_y(\cdot)$ are contributions from the roll and pitch dynamics. The rotational dynamic equation for r is given by

$$\dot{r} I_r(\theta, \phi) = M_z + \tau_r(F_x, F_y, \phi, \theta), \quad (23)$$

where $I_r(\cdot)$ is the moment of inertia associated with r, and $\tau_r(\cdot)$ is the additional external torques from the deflection of the center of mass of the chassis. The dynamic pitch equation is given by

$$\ddot{\theta} I_\theta(\phi) + D_\theta \dot{\theta} + K_\theta \theta = \tau_\theta(F_x, \phi, \theta) + \nu_\theta(r, \phi, \dot{\phi}, \theta, \dot{\theta}), \quad (24)$$

where $I_\theta(\cdot)$ is the moment of inertia associated with θ, $D_\theta \dot{\theta} + K_\theta \theta$ models a spring-damper system, $\tau_\theta(\cdot)$ is

external torques, and $\nu_\theta(\cdot)$ is the lower-order inertial terms. The dynamic roll equation is given by

$$\ddot{\phi} I_\phi(\phi,\theta) + D_\phi \dot{\phi} + K_\phi \phi = \tau_\phi(F_y,\phi,\theta) + \nu_\phi(r,\phi,\dot{\phi},\theta,\dot{\theta}), \tag{25}$$

where $I_\phi(\cdot)$ is the moment of inertia associated with ϕ, $D_\phi \dot{\phi} + K_\phi \phi$ models a spring-damper system, $\tau_\phi(\cdot)$ is external torques, and $\nu_\phi(\cdot)$ is the lower-order inertial terms.

The vertical force equilibrium is given by

$$F_{z,1} + F_{z,2} + F_{z,3} + F_{z,4} = mg. \tag{26}$$

The lateral load-transfer dynamics are given by

$$-(l_{y,1}F_{z,1} + l_{y,2}F_{z,2}) = K_\phi \phi/2 + D_\phi \dot{\phi}/2, \tag{27}$$

$$-(l_{y,3}F_{z,3} + l_{y,4}F_{z,4}) = K_\phi \phi/2 + D_\phi \dot{\phi}/2. \tag{28}$$

Finally, the longitudinal load-transfer dynamics are given by the relation

$$\sum_{i=1}^{4} l_{x,i}F_{z,i} = K_\theta \theta + D_\theta \dot{\theta}. \tag{29}$$

The numerical model parameters employed in the chassis and tire models are detailed in [2].

3 SCENARIOS

This section presents the maneuvering scenarios considered in this paper.

3.1 Left-Hand Turn Scenario

The first scenario considered is a left-hand turn. Initially, the vehicle starts at $(X_p, Y_p) = (0, -30)$ m. The deviation from the center line of the road lane is computed as

$$e = \sqrt{X_p^2 + Y_p^2} - R, \tag{30}$$

where R is the radius of the turn. A lane constraint is introduced as

$$|e| \leq e_{\max}, \tag{31}$$

where $e_{\max}$ is the half-width of the lane. The vehicle is considered to have regained control (and thus the maneuver is completed) when the deviation starts to decrease, *i.e.*, when $\dot{e} \leq 0$.

3.2 Double Lane-Change Scenario

The second scenario considered is a double lane-change situation. The track is modeled by defining maximum and minimum limits on the position Y_p that varies with the vehicle position X_p. This modeling introduces the following lane constraints in the optimization:

$$Y_p \leq Y_t(X_p), \tag{32}$$

$$Y_p \geq Y_b(X_p), \tag{33}$$

where Y_t is the top border and Y_b is the bottom border. Each border is modeled using two step-functions according to

$$Y_t(X_p) = a + c(H(X_p - X_{t1}) - H(X_p - X_{t2})), \tag{34}$$

$$Y_b(X_p) = -a + c(H(X_p - X_{b1}) - H(X_p - X_{b2})), \tag{35}$$

where a, c, X_{t1}, X_{t2}, X_{b1}, and X_{b2} are track parameters and H is the Heaviside step-function. The step-function is, for numerical computation reasons in the optimization, approximated as

$$H_{\text{soft}}(x) = 0.5\left(1 + \tanh\left(\frac{2\pi x}{\tau}\right)\right), \tag{36}$$

where τ is a parameter that determines the rise time of the step approximation. The track parameters are inspired by the ISO 3888 standard for a double lane-change maneuver, with some simplifications such as making all sections 3 m wide. In the official standard, the car has to pass between cones without moving them. To approximate this situation, while keeping the parameterization simple and only constraining the center of mass (X_p, Y_p), the size of the drivable area is made more narrow to account for the width of the car frame. The track is illustrated in the upper plot in Figure 3, where the more narrow borders are marked in red. The parameters used for the track are collected in Table 1.

Table 1.
Parameters used for the double lane-change track.
All of the parameter units are in meter.

A	12
B	13.5
C	11
D	12.5
E	12
w_{lane}	3
$w_{\text{car-frame}}$	1.7
τ	2
a	$(w_{\text{lane}} + w_{\text{car-frame}})/2$
c	$w_{\text{lane}} + 1$
X_{t1}	$A + \tau/2$
X_{t2}	$A + B + C + D - \tau/2$
X_{b1}	$A + B - \tau/2$
X_{b2}	$A + B + C + \tau/2$

3.3 Avoidance-Maneuver Scenario

The track used for modeling of the double lane-change scenario is also used to examine an avoidance scenario. The two scenarios in the same track differ only with regard to the constraint on the final state. While the double lane-change takes place on the complete track with two turns, the avoidance scenario only lasts until the initial obstacle has been avoided.

4 OPTIMAL CONTROL PROBLEM

To investigate the braking patterns under different conditions in the considered scenarios, an optimal control problem (OCP) was devised and subsequently solved. The optimization criterion was chosen as a weighted sum of the velocity when entering the maneuver and the velocity when exiting the same, to parameterize the trade-off between all-wheel braking and yaw-moment control. The initial-velocity criterion puts the vehicle in at-the-limit behavior, where road and vehicle constraints are the only limiting factors. For the final-velocity criterion, the initial velocity is still of importance, but apart from constraints there is an added penalty for decreasing the velocity.

Constraints on the control inputs u, *i.e.*, the wheel torques $T_{u,i}$ and steering angle δ, were introduced. The OCP over the time interval $[t_0, t_f]$ is stated mathematically as:

$$\begin{aligned}
\text{minimize} \quad & -\eta v_0 - (1-\eta) v_f && (37)\\
\text{subject to} \quad & T_{u,i,\min} \leq T_{u,i} \leq 0,\ i \in \{1,2,3,4\}, && (38)\\
& |\delta| \leq \delta_{\max}, \quad |\dot{\delta}| \leq \dot{\delta}_{\max}, && (39)\\
& F_c x(0) = x_0, \quad G_c x(t_f) = x_f && (40)\\
& f(X_p, Y_p) \leq 0, && (41)\\
& \dot{x} = G(x,y,u), \quad h(x,y,u) = 0, && (42)
\end{aligned}$$

where $0 \leq \eta \leq 1$, $v_0 = v(t_0)$ is the initial velocity, $v_f = v(t_f)$ is the final velocity, F_c a matrix with zeros and ones defining which states that have initial conditions, x_0 is the initial conditions, G_c a matrix with zeros and ones defining the states where terminal constraints exist, x_f is the desired final states, and $f(X_p, Y_p)$ is the lane constraint for the vehicle position (X_p, Y_p) in a global coordinate system. Note that changing only the single parameter η describes the full range of this optimization criterion that leads to the observations presented in Section 5. The chassis and tire models are formulated as a semi-explicit differential-algebraic equation (DAE) system, defined by the functions G and h, where y denotes the outputs. At the start of the maneuver, v_0 is a free parameter; the maneuver is terminated once the final state defined by x_f is reached.

Since numerical solutions for the OCP are intractable, direct collocation [9] was used to transform the problem into discrete time, resulting in a large nonlinear program (NLP) to be solved numerically. To this purpose, the optimization framework JModelica.org [10] was used together with the NLP-solver IPOPT [11] integrated with the linear solver HSL MA57 [12]. For further details regarding the overall solution methodology employed for the particular vehicle and chassis models, the reader is referred to [8].

5 RESULTS & DISCUSSION

The OCP defined in Section 4 was solved with varying weight η, with the initial guess in the iterative numerical optimization set to 50 km/h for v_0 and 4 s for t_f. No initialization of the trajectories of the model variables was required to solve the OCP. Note that the selection of the set of weights η for which the OCP was solved, is different for the three scenarios considered, the reason being to ensure that each scenario exhibits a variety of braking behaviors. In order to avoid unnecessary control actuation with the steering input, a small weight on the derivative of the steering angle is added by introducing the term $10^{-4} \int_0^{t_f} \dot{\delta}(t)^2 \, \mathrm{d}t$ in the cost function of the OCP. The leading constant is small enough, so as to not influence any examined quantitative or qualitative measures of the maneuvers.

5.1 Additional Evaluation Measures

The body slip β of the vehicle is used to evaluate the behaviors in the maneuvers, and this quantity is given by

$$\beta = \arctan\left(\frac{v_y}{v_x}\right). \tag{43}$$

Given the definition of the body slip, the force perpendicular to the direction of travel and path, $F_\perp$, is given by

$$F_\perp = F_y \cos(\beta) - F_x \sin(\beta). \tag{44}$$

The contribution to the yaw moment from the applied braking forces on a single wheel is given by the contribution of the longitudinal force together with the loss of lateral force due to longitudinal slip,

$$\Delta M_i = \begin{bmatrix} l_{x,i} & l_{y,i} \end{bmatrix} \begin{bmatrix} F_{x,i}\sin(\delta_i) + (F_{y,i} - F_{y0,i})\cos(\delta_i) \\ (F_{y,i} - F_{y0,i})\sin(\delta_i) - F_{x,i}\cos(\delta_i) \end{bmatrix}. \tag{45}$$

It is assumed that the braking forces of the wheels on the left side of the vehicle give a contribution to the moment toward the left, and the wheels on the right side similarly give a contribution toward the right. It is also interesting to study the total contribution from the braking forces of all wheels. The braking moments that will be studied in the analysis of the maneuvers are thus:

$$\Delta M_{\text{left}} = \Delta M_1 + \Delta M_3, \tag{46}$$

$$\Delta M_{\text{right}} = \Delta M_2 + \Delta M_4, \tag{47}$$

$$\Delta M = \Delta M_{\text{left}} + \Delta M_{\text{right}}. \tag{48}$$

5.2 Left-Hand Turn

The left-hand turn scenario is examined for a road radius of 30 m and a lane-width of 2 m. Figure 2 illustrates the scenario with a vehicle entering a turn at a velocity computed as the solution of the OCP, and selected vehicle trajectories are plotted for different values of the weight η. In the upper plot, the geometry

of the left-hand turn is plotted together with the vehicle paths, where dots mark the final vehicle positions. Since the vehicle slips further and further toward the edge of the lane during the maneuver, the curvature of the minimum required vehicle path to avoid leaving the lane increases.

Table 2 shows the initial velocity, the final velocity, and the resulting value of the cost function (37) in the OCP more clearly for each η. As can be observed in the differences in velocity trajectories v for the different optimal solutions, a higher entrance velocity requires significantly more braking action during the maneuver. With a higher initial velocity v_0, the vehicle is subject to more lateral slip, and thus the vehicle path will have a higher final curvature. The final velocity v_f is limited by the available lateral tire forces and the maximum curvature of the vehicle path. Applying heavy braking forces to reduce the velocity, of course, produces even more lateral slip.

Table 2.
Results for the left-hand turn scenario with variations of η, where J is the value of the optimization criterion in (37).

η	v_0 [km/h]	v_f [km/h]	J [km/h]
1	65.6	47.7	65.6
2/3	65.1	50.5	60.2
1/2	64.5	51.4	57.9
1/6	62.1	52.4	54.0
0	60.7	52.6	52.6

Moreover, in Figure 2 it can be observed in the plot of the steering angle δ that the steering rate $\dot{\delta}$ is in all cases saturated from the start of the maneuver until $t \approx 0.25$ s. Lateral tire forces may also be delayed as a result of the relaxation length of the tires, see the relation (8). This behavior tells us that additional turn-in moment most likely would be beneficial. The moment ΔM resulting from the applied braking torques on the wheels is thus of interest. Depending on the weights in the cost function of the optimization, ΔM is either a turn-in moment, a turn-out moment, or its sign varies with time. Note that the total moment M_z is for all cases primarily a turn-in moment. The moment from the applied braking torques is further split into two parts, depending on which side of the vehicle they act on. Torques applied to the outer wheels produce a turn-out yaw moment ΔM_{right} that is heavily dependent on the initial velocity. For $\eta = 1/6$, there is even a different strategy where the solution seems to wait for the turn-in moment to build up before applying any braking torques on the outer wheels. For $\eta = 0$, similar to a traditional yaw-control strategy, no torque is applied on the outer wheels.

Torques applied on the inner wheels produce the moment ΔM_{left}. This turn-in yaw moment can be seen to be significantly independent of the initial velocity, only when the vehicle starts to experience over-steer the solutions are different. The peak observed in the plot of ΔM_{left} in Figure 2 is limited by the available longitudinal friction forces of the tires. The rise and sink times of the peak are limited by the first-order dynamics between the commanded and the actual wheel torque. A cost that comes with applying more braking forces in addition to generating a turn-out moment is that there are less lateral forces available, which can be seen in the plot of the force lateral to the path, $F_\perp$, in Figure 2. As the vehicle is subject to oversteering most of the time during the maneuver, the additional turn-out moment does help to contribute to a lower body slip β.

5.3 Double Lane-Change

The double lane-change scenario is examined for the parameters given in Table 1, with the initial position of the vehicle being $(X_p, Y_p) = (10, 0)$ m, and the final position $(X_p, Y_p) = (61, 0)$ m. Figure 3 illustrates the situation considered, with selected vehicle trajectories plotted for different values of the weight η. In the upper plot, the double lane-change track is plotted together with the vehicle paths for the respective value of the weight. The road edges are plotted in black, while the road constraints that take the vehicle width into account are plotted in red. The path for $\eta = 0$ does not touch the upper boundary during the middle section of the track and is thus only limited by the road constraint at $X_p = 25.5$ m and 49 m.

Table 3 shows the initial velocity, the final velocity, and the resulting value of the cost function (37) in the OCP for each η. Observing the velocity v and the perpendicular force $F_\perp$ in Figure 3 closer, the final velocity seems to be restricted by the right-hand turn at around $t \approx 1.5$–2 s. At that time the perpendicular force is the limiting quantity and for the rest of the maneuver, the decrease in velocity is minor. During the initial left turn, the body slip β is primarily negative, which corresponds to an oversteer behavior. At the second turn to the right, the solutions obtained for all weights but $\eta = 1$ show an over-steer behavior in β, but where the vehicle is driving very slowly.

Table 3.
Results for the double lane-change scenario with variations of η, where J is the value of the optimization criterion in (37).

η	v_0 [km/h]	v_f [km/h]	J [km/h]
1	62.9	28.0	62.9
2/3	62.0	36.8	53.6
1/2	59.6	43.1	51.4
1/3	58.0	44.7	49.1
0	54.7	45.7	45.7

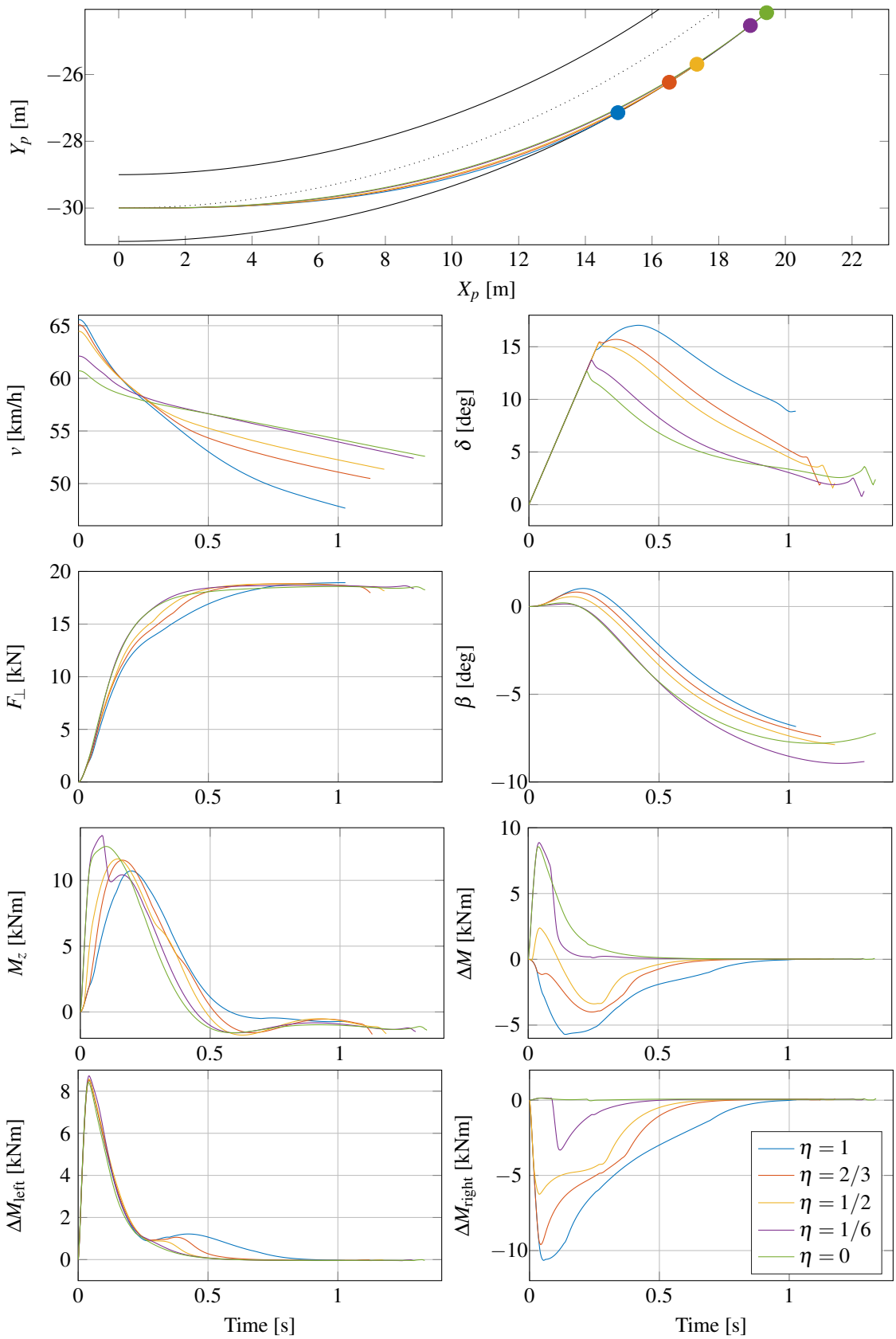

Figure 2. Optimal trajectories for different weights η when entering a turn with radius 30 m and width 2 m: v, vehicle velocity; δ, steering angle; $F_\perp$, force perpendicular to direction of travel; β, body slip; M_z, total moment; ΔM, moment resulting from braking torques; ΔM_{left}, turn-in moment resulting from braking torques; ΔM_{right}, turn-out moment resulting from braking torques.

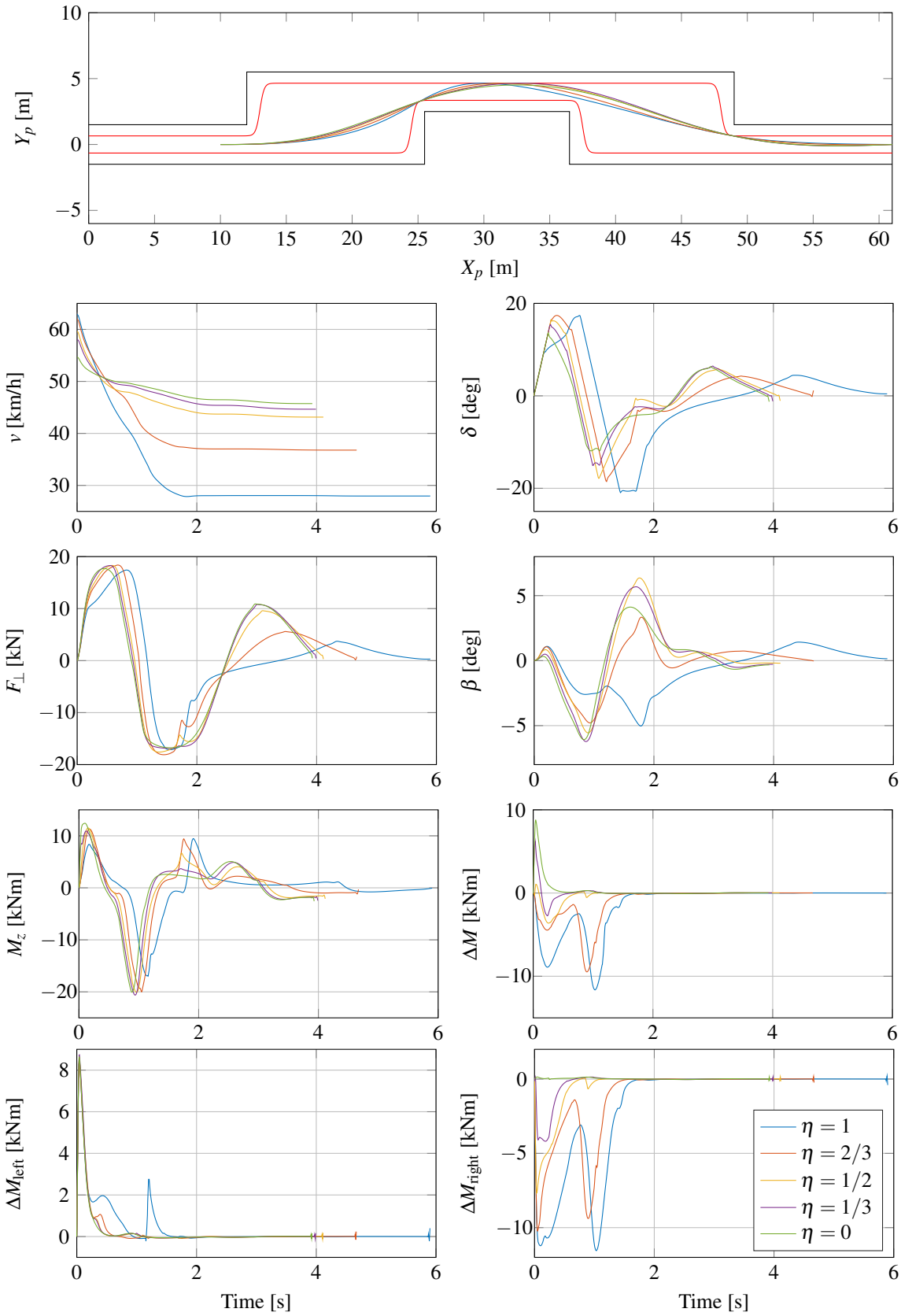

Figure 3. Optimal trajectories for different weights η when performing a double lane-change maneuver: v, vehicle velocity; δ, steering angle; $F_\perp$, force perpendicular to direction of travel; β, body slip; M_z, total moment; ΔM, moment resulting from braking torques; ΔM_{left}, turn-in moment resulting from braking torques; ΔM_{right}, turn-out moment resulting from braking torques.

From the plot of the steering angle δ in Figure 3, it is clear that the steering rate $\dot{\delta}$ is saturated for a large part of the maneuver before $t = 1.5$ s. During the first second of the maneuver, the moments ΔM resulting from the applied braking torques are very similar to those in the left-hand turn in Figure 2. For the plotted solutions with weights $\eta \geq 1/2$, additional turn-in moment is generated during the right turn by braking the wheels on the right side of the vehicle, as can be seen in the plot of ΔM_{right}. Further, in the plot of the optimal trajectory for ΔM_{left} with $\eta = 1$ in Figure 3, it can be seen that the vehicle brakes the wheels on the left side during the turn to the right. This behavior may be more or less pronounced for values of η close to 1, since the final velocity is only to a small extent, or not at all, penalized, which in turn allows solutions with more or less braking being fairly close in the value of the cost function in the OCP.

5.4 Avoidance Maneuver

The avoidance-maneuver scenario is examined in the same track as the double-lane change, using the parameters given in Table 1, with the same initial position $(X_p, Y_p) = (10, 0)$ m as in the double lane-change situation, but the final position chosen at the edge of the first obstacle at $X_p = 25.5$ m without any specified Y_p coordinate. The upper plot in Figure 4 illustrates the scenario considered, with the same track as in Figure 3, but different resulting vehicle paths. In addition, selected vehicle trajectories are shown.

Table 4 shows the initial velocity, the final velocity, and the resulting value of the cost function (37) in the OCP for each η. Comparing with the double lane-change maneuver in Table 3, the initial velocity v_0 has increased, significantly so for low weights η. With a lower velocity difference, the differences in the geometric paths are also smaller. Despite the higher approach angle for the second turn, this observed behavior suggests that for this specific track, braking strategies obtained with high values of η are more resilient to future road constraints.

Table 4.
Results for the avoidance-maneuver scenario with variations of η, where J is the value of the optimization criterion in (37).

η	v_0 [km/h]	v_f [km/h]	J [km/h]
1	63.7	42.6	63.7
5/6	63.3	47.8	60.8
2/3	62.5	50.3	58.4
1/2	61.6	51.6	56.6
0	59.3	52.9	52.9

At the end of the maneuver, it can from the rapidly decreasing steer angle δ and the negative total moment M_z in Figure 4 be observed that for most of the solutions obtained with different η, the vehicle reduces its turning rate. The reason may be to reduce the lateral force by straightening out the path in order to maintain velocity. Comparing with the initial turn in the double lane-change maneuver in Figure 3 and with the left-hand turn in Figure 2, the striking similarities are clear.

5.5 Parameterization Behavior

In this section, implications on the braking behavior from the optimization cost function in (37) are studied in light of all the scenarios considered and some of the related research.

Because of limited lateral forces, both velocity quantities in the cost function are in all cases limited by the turning radius, and will thus promote paths with a large turning radius. Accelerating maneuvers are not covered in this paper, but in [4] it is concluded that the maximum exit velocity case, $\eta = 0$ in the setting of this paper, results in a maximum radius trajectory at the exit of a turn. In the mirrored case for braking maneuvers covered here, increasing the initial velocity requires a larger turning radius at the beginning of the maneuver before the vehicle has decreased its velocity sufficiently much. In the case of a single turn as in Figures 2 and 4, the initially larger turning radius is penalized with a smaller turning radius during the later part of the turn. When also considering a subsequent right-hand turn in a lane-change maneuver, constrained by a boundary region as in Figure 3, a large initial turning radius also causes a smaller maximum turning radius during the second turn.

For all the scenarios considered, it holds that with $\eta = 0$ braking is only used to generate an initial turn-in moment. After the initial phase, only steering action is used. When increasing the weight η, more braking forces are added that contribute both to turn-in and turn-out moments. For intermediate values of η, there are solutions where the initial turn-in moment is kept, and then changed to a turn-out moment later in the turn. This is similar to how a yaw-control strategy may perform, with the difference that here these solutions mean braking with wheels on both sides of the vehicle at the same time.

For the scenarios considered in this paper, it can be observed that to limit the body slip β using braking forces it would be desirable to produce a turn-out moment, since in relation to β the vehicle oversteers. In [2], [5], limiting the body slip is concluded to have a small impact on the performance of a braking strategy for a single-turn scenario. Low-braking strategies with low values of η mostly utilize turn-in moment, which stand in conflict with reducing the body slip β.

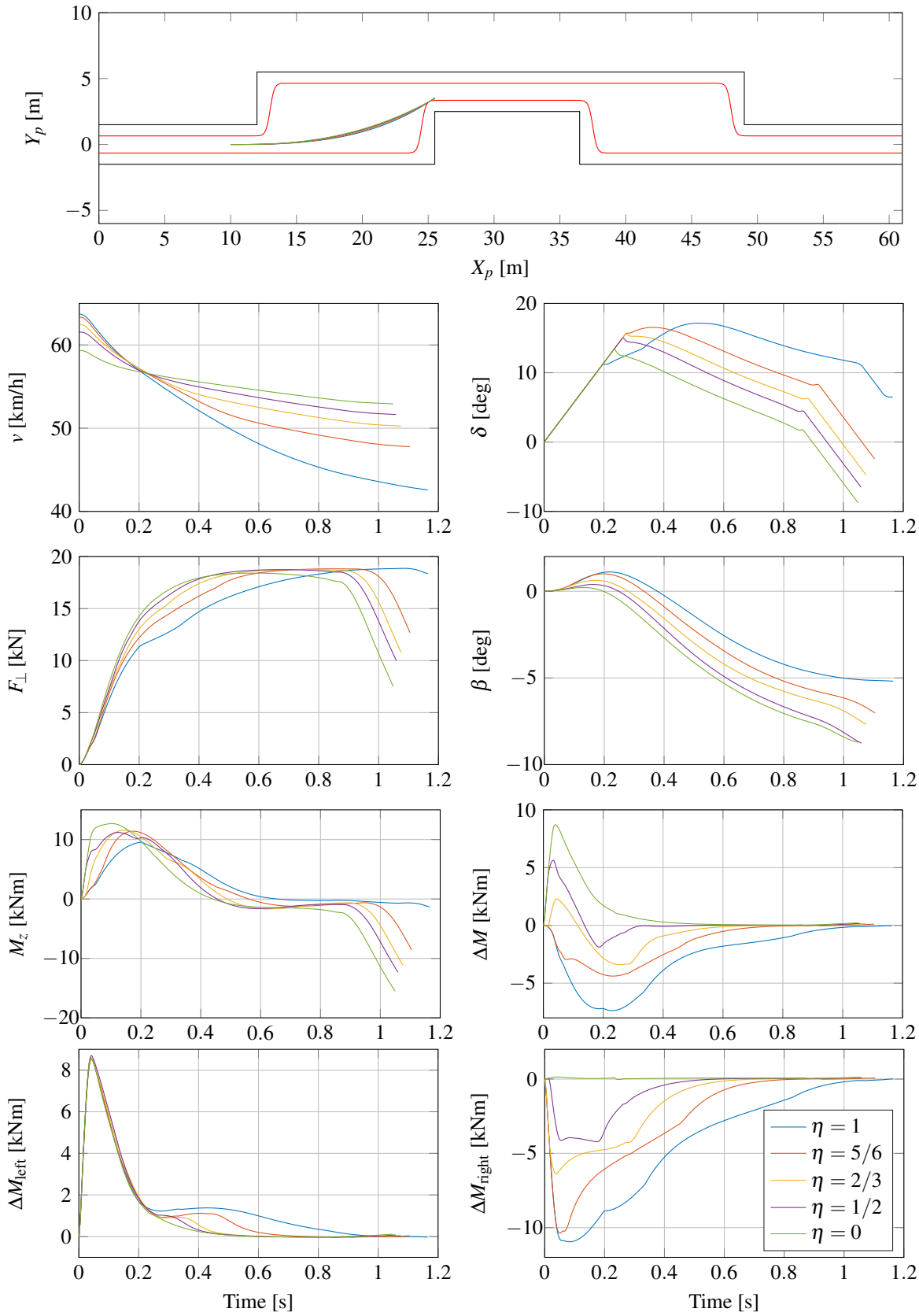

Figure 4. ***Optimal trajectories for different weights η when performing an avoidance maneuver: v, vehicle velocity; δ, steering angle; $F_\perp$, force perpendicular to direction of travel; β, body slip; M_z, total moment; ΔM, moment resulting from braking torques; ΔM_{left}, turn-in moment resulting from braking torques; ΔM_{right}, turn-out moment resulting from braking torques.***

6 CONCLUSIONS

In this paper, different braking patterns and behaviors in time-critical situations were investigated. The cost function in the optimization was parametrized in a weight η. For $\eta = 1$, solutions close to a pure lane-keeping strategy are obtained—*i.e.*, heavy braking on all wheels to reduce the velocity given the available tire friction. Decreasing the weight η, in contrast leads to solutions closer to traditional yaw control, where the majority of the braking is applied on the inner wheels (see Figure 2). This behavior also holds true when increasing the complexity of the maneuver (see Figures 3 and 4). From the investigated OCP formulation, the benefits of a lane-keeping strategy are immediate, both in terms of the maximum possible initial velocity and the velocity reduction. It also provides an approach for analyzing and understanding the relation between traditional yaw control and optimal lane-keeping for autonomous vehicles, since it embeds these strategies as the end-point values of the interpolation parameter, and adds a continuous family of behaviors in between.

REFERENCES

[1] R. Rajamani, *Vehicle Dynamics and Control*, 2nd. New York, United States: Springer, 2012.

[2] K. Lundahl, B. Olofsson, K. Berntorp, J. Åslund, and L. Nielsen, "Towards lane-keeping electronic stability control for road-vehicles," in *Proc. 19th IFAC World Congress*, Cape Town, South Africa, 2014, pp. 6319–6325.

[3] P. Sundström, M. Jonasson, J. Andreasson, A. Stensson Trigell, and B. Jacobson, "Path and control signal optimisation for over-actuated vehicles in two safety-critical maneuvers," in *10th Int. Symp. on Advanced Vehicle Control (AVEC 10)*, Loughborough, United Kingdom, 2010.

[4] E. Velenis and P. Tsiotras, "Minimum time vs. maximum exit velocity path optimization during cornering," in *Proc. IEEE Int. Symp. on Industrial Electronics (ISIE)*, Dubrovnik, Croatia, 2005, pp. 355–360.

[5] M. Klomp, M. Lidberg, and T. J. Gordon, "On optimal recovery from terminal understeer," *Proc. Institution of Mechanical Engineers, Part D: Journal of Automobile Engineering*, vol. 228, no. 4, pp. 412–425, 2014.

[6] K. Berntorp, "Derivation of a six degrees-of-freedom ground-vehicle model for automotive applications," Department of Automatic Control, Lund University, Sweden, Technical Report 7627, 2013.

[7] H. B. Pacejka, *Tyre and Vehicle Dynamics*, 2nd. Oxford, United Kingdom: Butterworth-Heinemann, 2006.

[8] K. Berntorp, B. Olofsson, K. Lundahl, and L. Nielsen, "Models and methodology for optimal trajectory generation in safety-critical road–vehicle manoeuvres," *Vehicle System Dynamics*, vol. 52, no. 10, pp. 1304–1332, 2014.

[9] L. T. Biegler, A. M. Cervantes, and A. Wächter, "Advances in simultaneous strategies for dynamic process optimization," *Chemical Engineering Science*, vol. 57, pp. 575–593, 2002.

[10] J. Åkesson, K.-E. Årzén, M. Gäfvert, T. Bergdahl, and H. Tummescheit, "Modeling and optimization with Optimica and JModelica.org—Languages and tools for solving large-scale dynamic optimization problems," *Computers and Chemical Engineering*, vol. 34, no. 11, pp. 1737–1749, 2010.

[11] A. Wächter and L. T. Biegler, "On the implementation of an interior-point filter line-search algorithm for large-scale nonlinear programming," *Mathematical Programming*, vol. 106, no. 1, pp. 25–57, 2006.

[12] *HSL. A collection of Fortran codes for large scale scientific computation*, `http://www.hsl.rl.ac.uk/`, Accessed: 2017-02-15.